

Mechanistic Insight into Iron-Catalyzed C-H Bond Activation and C-C Coupling

Samantha M. Brewer,^a Timothy M. Schwartz,^a Magy A. Mekhail,^a Lara S. Turan,^a Timothy J. Prior,^b Timothy J. Hubin,^c Benjamin G. Janesko,^a and Kayla N. Green^{*a}

^aDepartment of Chemistry and Biochemistry, Texas Christian University, 2950 S. Bowie, Fort Worth, TX 76129, United States.

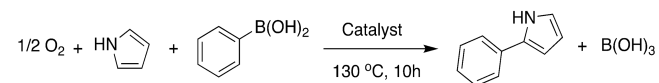
^bDepartment of Chemistry and Positron Emission Tomography Research Centre, University of Hull, Cottingham Road, Hull HU6 7RX, UK.

^cDepartment of Chemistry and Physics, Southwestern Oklahoma State University, 100 Campus Drive, Weatherford, OK 73096, United States.

ABSTRACT: Iron-catalyzed C-C coupling reactions of pyrrole provide a unique alternative to the traditional Pd-catalyzed counterpart. However, many details regarding the actual mechanism remain unknown. A series of macrocyclic iron(III) complexes were used to evaluate specifics related to the role of O₂, radicals, and μ-oxodiiron complex participation in the catalytic cycle. It was determined that the mononuclear tetra-azamacrocyclic complex is a true catalyst and not a stoichiometric reagent, while more than one equivalent of a sacrificial oxidant is needed. Furthermore, the reaction does not proceed through an organic radical pathway. μ-oxodiiron complexes are not involved in the main catalytic pathway, and the dimers are, in fact, off-cycle species that decrease catalytic efficiency.

INTRODUCTION

The discovery of Pd-catalyzed C-C cross coupling reactions, more commonly known today as Suzuki Miyaura coupling, in 1979 represented an important leap forward in terms of chemical synthesis.¹⁻² Using this chemistry, a newly formed C-C bond typically originates from an aryl halide and an organoborane. In recent years, however, there has been a push towards investigating Fe-catalyzed C-C coupling reactions as a means of achieving less toxic and cheaper catalytic processes compared to Pd.³⁻⁷ These virtues are vigorously debated because toxicity depends on the identity of the metal salts, as well as the type of toxicity measured.⁸ Additionally, the cost of the supporting ligands can offset the overall cost of the metal catalyst.⁹ Nonetheless, there is a strong cohort to further assert that Fe-based catalysis is important, and should be investigated further, because the electronics of base metals differ from their precious metal counterparts.¹⁰



Scheme 1. General reaction for the coupling of phenylboronic acid and pyrrole.

Within the scope of Fe-based catalysis, direct C-C coupling reactions facilitated by iron have been pioneered by Wen and co-workers.¹¹ Using tetra-azamacrocycles and iron salts, pyridine and pyrrole were independently coupled with phenylboronic acid to produce 2-phenylpyridine (41%) and 2-phenylpyrrole (66%), respectively (Scheme 1). The coupling of pyridine and phenylboronic acid was performed in the presence of an iron(III) salt. Conversely, pyrrole coupling to phenylboronic acid was performed using an iron(II) salt. Wen and co-workers proposed a mechanism for the iron(II)-catalyzed coupling of pyrrole and phenylboronic acid. In this mechanism, the iron(II) complex enters that catalytic cycle and is activated by oxygen to form an Fe-O species. The Fe-O species is proposed to activate the C₂-H bond of pyrrole. Following the report by Wen and co-workers, Dong *et al.* showed through mass spectrometry that an iron(III)-oxo species is present in the iron(III)-catalyzed C-C coupling of pyridine and phenylboronic acid.¹² An Fe(III)/Fe(I) process was proposed based on a computational study that began with the iron(III)-oxo species. Our team has shown that aza-macrocycles are broadly capable of catalyzing this reaction as well.^{4,5} Previous work also showed that the tetra-azamacrocycle alone, as well as Fe(ClO₄)₃ alone, produce either no, or trace amounts of, 2-phenylpyrrole.¹³⁻¹⁴ However, there still exists major deficiencies in the understanding of the mechanism, which can be addressed by the following questions: (1)

Do the iron(III) complexes act as stoichiometric reagents to afford C-C coupling type reactions? 2) Does oxygen oxidize pyrrole or the metal center? (3) What type of interaction does oxygen have with iron(III) catalysts? (4) Are any off-cycle species formed that may decrease catalytic efficiency?

In the current study, we sought to determine a more detailed understanding of the iron-catalyzed C-C coupling process from four viewpoints: (1) The need for oxygen atoms was investigated by altering the reaction conditions to eliminate all sources of oxygen, including dioxygen, water, and oxy-containing counter-ions, (2) the role of oxygen was investigated by determining if 3-pyrroline-2-one could serve as a starting material in the production of 2-phenylpyrrole, (3) the potential for a radical participation was tested by varying the radical scavenging ability of the catalyst used, (4) the role of μ -oxodiiron complexes under reaction conditions was further studied using absorbance spectroscopy.

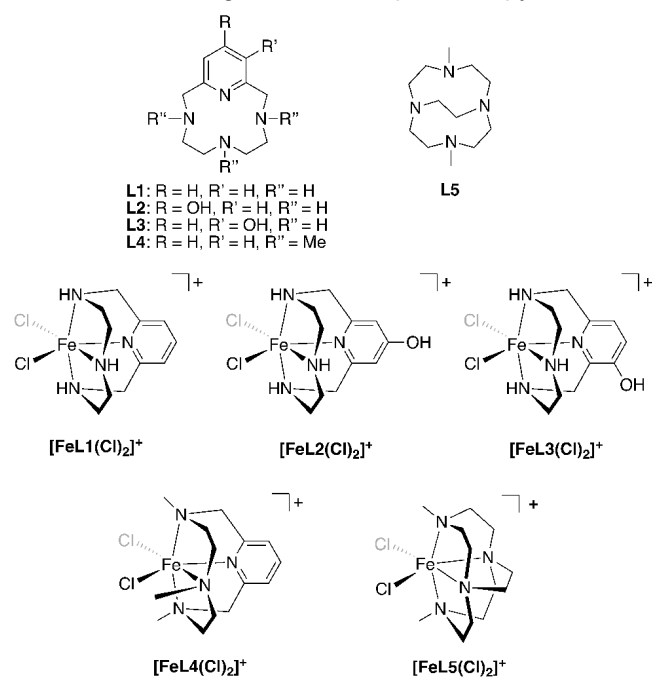


Figure 1. Chemical structure of ligands **L1-L5** and complexes **[FeL1-L5(Cl)₂]⁺**.

Table 1. Catalytic yields used to determine the need for oxygen in the coupling reaction described in Scheme 1.

Loading	Catalyst	Oxidant	% Yield
10%	[FeL2(Cl) ₂]Cl	air	58 ± 7 ^a
100%	[FeL2(Cl) ₂]ClO	*	16 ± 4
	⁴		
100%	[FeL2(Cl) ₂]Cl	*	Trace

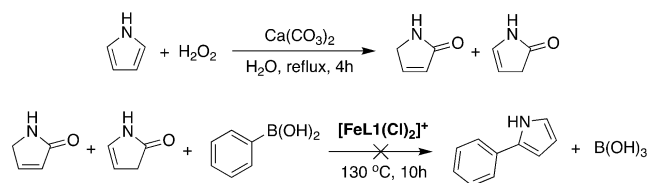
*excluded, ^aref.¹³

RESULTS

To determine if the iron-complexes act as a stoichiometric reagent in the C-C coupling between pyrrole and phenylboronic acid type coupling, the iron complex **[FeL2(Cl)₂]Cl** was tested for the ability to produce 2-phenylpyrrole in the absence of oxygen. When **[FeL2(Cl)₂]Cl** was loaded at 100 mol% and the reaction was heated for 10 h under anaerobic conditions (Table 1) no 2-phenylpyrrole was detectable. Therefore, the coupling only occurs in the presence of an oxygen source, and a stoichiometric pathway does not need to be included in the catalytic mechanism. Interestingly, the use of **[FeL2(Cl)₂]ClO₄** at 100% loading under anaerobic conditions resulted in 16 ± 4% product formation, indicating that the perchlorate counter-ion is capable of acting as sacrificial oxidant in iron catalysis. Although the perchlorate counter-ion was able to act as a sacrificial oxidant, a 1:1 mole ratio of perchlorate to iron was not sufficient to produce comparable yields to those obtained when 10 mol% **[FeL2(Cl)₂]Cl** was used open to air (58 ± 7%).¹³ This can be explained in two ways: 1) the perchlorate is not as effective an oxidant as air and 2) more than one equivalent oxidant is required to facilitate one turnover. The latter is consistent with experimental and computational studies that show Fe-C and Fe-Aryl do not spontaneously eliminate.¹⁵⁻¹⁶ Rather, the oxidation of the metal center triggers the elimination step and regeneration of the active catalyst. This would be a slight modification to the computationally derived mechanism proposed by Dong and co-workers where the product is released, followed by oxidation via O₂.¹⁷ It does not appear that this oxidation dependent reductive elimination was explored in their calculations but our results support the concomitant oxidation and product release.

The role of oxygen in the catalytic cycle

After establishing the need for an oxidant, an alternative mechanism to metal oxidation was considered. Specifically, pyrrole has been shown to oxidize to 3-pyrroline-2-one; therefore, oxidation of the reagent prior to entering the catalytic cycle was explored.¹⁴ To evaluate this, 3-pyrroline-2-one was independently synthesized via a previously reported procedure in which hydrogen peroxide is used to oxidize pyrrole in the presence of Ca(CO₃)₂ (Scheme 2).¹⁸ No 2-phenylpyrrole was isolated when 3-pyrroline-2-one was combined with phenylboronic acid in the presence of **[FeL1(Cl)₂]Cl** indicating this is not an intermediate in the catalytic mechanism. Therefore, based on these results, oxygen is required for oxidation chemistry with the iron and not the pyrrole substrate.



Scheme 2. Synthesis of 3-pyrroline-2-one as a potential starting material for pyrrole and phenylboronic acid coupling. 2-phenylpyrrole is not produced when $[\text{FeL2}(\text{Cl})_2]\text{Cl}$ was used for catalysis.

Radical participation

Many catalytic processes progress through a mechanism involving radical ions.¹⁹⁻²⁰ For example, Dantignana and co-workers recently reported hydrogen atom abstraction chemistries with the iron complex of **L4** that involves a carbon-centered radical.²¹⁻²² Based on this knowledge, the catalytic coupling of pyrrole with phenylboronic acid was evaluated to determine if a radical species is involved. Previously, the ligands **L1**, **L2**, and **L3** (Figure 1) were tested for radical scavenging ability using the DPPH (2,2-diphenyl-1-picrylhydrazyl) assay, which allows for analysis of a molecule's radical scavenging ability in solution.²³ An intense purple solution is obtained with a corresponding absorbance band at 515 nm when DPPH is dissolved in EtOH.²⁴⁻²⁶ The intensity of the absorbance band is concentration dependent and decreases as radical scavenging systems react with DPPH through a hydrogen atom transfer (HAT) type reaction. Quantification of radical scavenging ability for a compound of interest is obtained by comparison to a positive control such as BHT (2,6-di-tert-butyl-4-methylphenol). Ligands **L2** and **L3** were previously shown to be potent radical scavengers, but **L1** did not show any reactivity.²⁷⁻²⁸ The radical scavenging activity of **L2** and **L3** was attributed to the pyridol moiety, which scavenges radicals in a similar manner to tannins.²⁹ However, the radical scavenging activity of metal congeners has not been explored to date. Therefore, a DPPH assay was performed with $[\text{FeL1}(\text{Cl})_2]^+$, $[\text{FeL2}(\text{Cl})_2]^+$, and $[\text{FeL3}(\text{Cl})_2]^+$ (Figure 2); complex $[\text{FeL1}(\text{Cl})_2]^+$ did not scavenge radicals at or below 0.75 mM. In contrast, $[\text{FeL2}(\text{Cl})_2]^+$ and $[\text{FeL3}(\text{Cl})_2]^+$ provided concentration-dependent radical scavenging activity at concentrations greater than 250 μM .

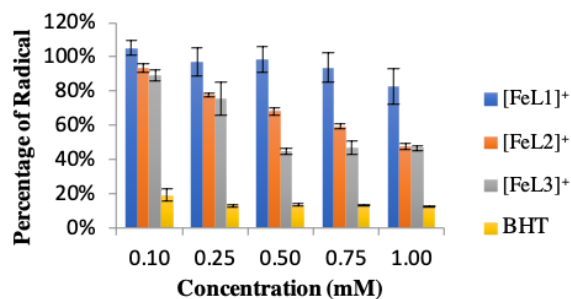


Figure 2. DPPH assay showing radical scavenging ability relative to radical remaining for $[\text{FeL1}(\text{Cl})_2]\text{ClO}_4$, $[\text{FeL2}(\text{Cl})_2]\text{ClO}_4$, and $[\text{FeL3}(\text{Cl})_2]\text{ClO}_4$.

The catalytic yields obtained in the presence of 198 mM $[\text{FeL1}(\text{Cl})_2]^+$, $[\text{FeL2}(\text{Cl})_2]^+$, and $[\text{FeL3}(\text{Cl})_2]^+$ were compared to the radical scavenging ability of each complex. Complex $[\text{FeL1}(\text{Cl})_2]^+$, $[\text{FeL2}(\text{Cl})_2]^+$, and $[\text{FeL3}(\text{Cl})_2]^+$ afforded $57 \pm 3\%$, $58 \pm 7\%$, and $52 \pm 7\%$ 2-phenylpyrrole¹³ and a 0%, 50%, and 50% reduction of the DPPH radical, respectively. In addition, 10% and 100% loading of BHT, with respect to phenylboronic acid, showed no difference in product yield. If an organic radical were present, the iron complexes of **L2** and **L3** would have resulted in lower catalytic yields due to quenching of an organic radical intermediate. Therefore, the DPPH results indicate that an organic radical ion is not likely present in the reaction mechanism.

Table 2. DFT-computed reaction energies ΔE (eV) for two representative one-electron oxidations of high-spin $\text{Fe}^{\text{III}}\text{L}$ complexes: (a) $[\text{Fe}^{\text{III}}\text{L}(\text{Cl})\text{OH}]^+ + 1/2 \text{H}_2\text{O}_2 \rightarrow [\text{Fe}^{\text{IV}}(\text{=O})\text{Cl}]^+ + \text{H}_2\text{O}$ (b) $[\text{Fe}^{\text{III}}\text{L}(\text{Cl})_2]^+ + \text{H}_3\text{O}^+ + 1/2 \text{H}_2\text{O}_2 \rightarrow [\text{Fe}^{\text{IV}}\text{L}(\text{Cl})_2]^{2+} + 2 \text{H}_2\text{O}$.

	L1	L2	L3
(a) $\text{Fe}^{\text{IV}}(\text{=O})$	-0.01	-0.02	-0.07
(b) Fe^{IV}	-0.05	-0.19	-0.43

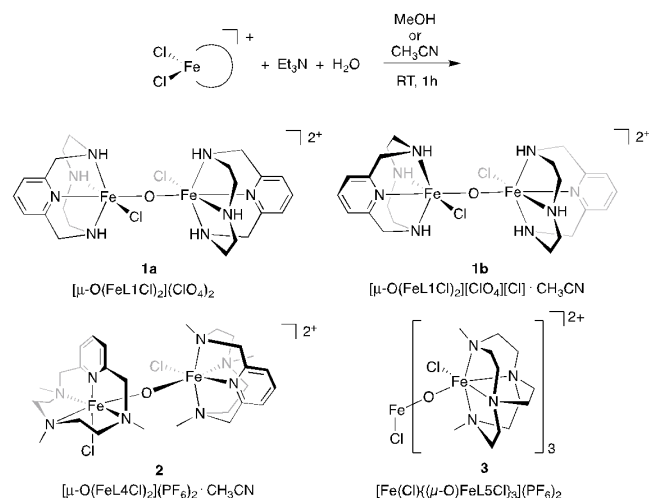
Calculations use Kohn-Sham density functional theory with the B3LYP exchange-correlation functional, the def2-TZVPP basis set, and the SMD continuum model for water solvent. Other approximations give qualitatively similar results as noted in Supporting Information.

Given the results of the DPPH experiments and reports of the **FeL4** complex accessing both $\text{Fe}^{\text{IV}}(\text{=O})$ and $\text{Fe}^{\text{V}}(\text{=O})$ states²¹, computational studies were carried out to evaluate the potential for an $\text{Fe}(\text{IV})$ -oxo species to form within the series and how the changes in ligand substitution impacted the stability of this complex. These high valent species have not been discussed in previously proposed mechanisms and were, therefore, considered here.¹³⁻¹⁴ Table 2 shows that the DFT computed reaction energies for forming $[\text{Fe}^{\text{IV}}(\text{=O})\text{LCI}]^+$

complexes (reaction (a), supporting information) are essentially the same (within 0.1 eV with B3LYP/def2-tzvp) for **L1**, **L2**, and **L3**. This is consistent with catalytic results, where the complexes provide similar product yields; i.e. the stability of the high-valent iron oxidation state is independent of the substitutions explored in this series. These results are also consistent with previous spectroscopic studies of the **FeL4** complex, which can access both $\text{Fe}^{\text{IV}}(\text{=O})$ and $\text{Fe}^{\text{V}}(\text{=O})$ states, the latter of which is a more efficient HAT catalyst.²¹ DFT-predicted oxidation energies without an oxo-ligand (reaction (b)) are markedly varied within the series. Without an oxygen ligand, oxidation is predicted to occur at Cl or L ligands, not at the metal. Other levels of theory give similar predictions (Supporting Information). Overall radical scavenging studies and DFT simulations suggest that a high-valent $\text{Fe}(\text{=O})$ pathway should be considered.

Implication and participation of μ -oxodiiron complexes in C-C coupling reactions

μ -Oxodiiron complexes are known to play a role in oxygen atom transfer reactions, but their role in C-C coupling reactions has not been established.³⁰⁻⁶⁵ The complexes $[\text{FeL1}(\text{Cl}_2)]^+$, $[\text{FeL4}(\text{Cl}_2)]^+$, and $[\text{FeL5}(\text{Cl}_2)]^+$ were explored due to the well-documented facile formation of μ -oxodiiron complexes in solutions with a pH above 1.⁶⁶⁻⁶⁸ $[\text{FeL4}(\text{Cl}_2)]^+$ and $[\text{FeL5}(\text{Cl}_2)]^+$ (Figure 1) were added to the series to explore the impact of steric bulk on the N-atoms because it was hypothesized that the steric bulk in ligands **L4** and **L5** would impact the formation or stability of the μ -oxodiiron complexes. In the presence of Et_3N and H_2O , $[\text{FeL1}(\text{Cl}_2)]^+$ and $[\text{FeL4}(\text{Cl}_2)]^+$ readily formed μ -oxodiiron complexes **1** and **2** (Scheme 3). However, $[\text{FeL5}(\text{Cl}_2)]^+$ formed an unexpected tetrametallic species **3** (Scheme 3) that was isolated in small quantities and studied by X-ray diffraction.



Scheme 3. Synthesis of structures of **1a**, **1b**, and **2** dimers, as well as **3** tetrametallic species.

The inability of $[\text{FeL5}(\text{Cl}_2)]^+$ to form the well-known, stable diiron species under basic conditions expands on previous reports that dimer formation is not observed upon oxidation of the iron(II) complex to the iron(III) in the presence of O_2 .^{66-67, 69} This observation is attributed to the additional steric bulk on the N-atoms. The triply- μ -oxo bridged species (**3**) proved to be extremely unstable in our hands. The participation of a μ -oxo dimer in the catalytic mechanism is unlikely because increased catalytic yields ($74\% \pm 3$) were observed with $[\text{FeL5}(\text{Cl}_2)]^+$ compared to $[\text{FeL1}(\text{Cl}_2)]^+$ and $[\text{FeL4}(\text{Cl}_2)]^+$.⁷⁰ The μ -oxo complexes **1** and **2** (Figure 3) were characterized by single crystal X-ray diffraction, NMR, and absorbance spectroscopy, which are discussed in depth below. Moreover, the absorbance spectra of $[\text{FeL1}(\text{Cl}_2)]^+$ and $[\text{FeL4}(\text{Cl}_2)]^+$ in the presence of pyrrole showed the formation of **1** and **2**. Therefore, **1** and **2** are assigned as off-cycle species that decrease catalytic yields of $[\text{FeL1}(\text{Cl}_2)]^+$ and $[\text{FeL4}(\text{Cl}_2)]^+$.

Reactivity of $[\text{FeL1}(\text{Cl}_2)]^+$, $[\text{FeL4}(\text{Cl}_2)]^+$, and $[\text{FeL5}(\text{Cl}_2)]^+$ with Et_3N and H_2O

As noted above, $[\text{FeL1}(\text{Cl}_2)]^+$, $[\text{FeL4}(\text{Cl}_2)]^+$, and $[\text{FeL5}(\text{Cl}_2)]^+$ were treated with Et_3N in the presence of H_2O in either MeOH ($[\text{FeL1}(\text{Cl}_2)]^+$) or CH_3CN ($[\text{FeL4}(\text{Cl}_2)]^+$ and $[\text{FeL5}(\text{Cl}_2)]^+$) as shown in Scheme 3. Dimers **1** ($[\mu\text{-O}(\text{FeL1Cl})_2]^{2+}$) and **2** ($[\mu\text{-O}(\text{FeL4Cl})_2]^{2+}$), as well as, **3** ($[\text{Fe}(\text{Cl})(\mu\text{-O})\text{FeL5Cl}]_3^{2+}$) were isolated from the reaction mixtures as single crystals suitable for diffraction studies.

Complex **1** crystallized in two separate forms, **1a** and **1b**, depending on the solvent used for crystal growth. Due to the small amount (3 mg) of **3** isolable, the only characterization successfully completed was X-ray crystallography.

Solid-state structure determination of **1**, **2**, and **3**

The solid-state structures of **1a**, **1b**, **2**, and **3** are shown in Figures 3-4. Crystals of **1a** were obtained by slow evaporation of MeOH; isolation of the crystals suitable for X-ray diffraction resulted in a 50% yield. The crystals of **1a** were dark brown with a brick morphology. Several unsuccessful attempts were made to slow the crystallization process, to eliminate the presence of disorder, twinning, and pseudo-symmetry observed when crystals were grown by slow evaporation at room temperature. The twinning and pseudo-symmetry were identified using the program PLATON. The crystal structure of **1a** was refined in the space group C2/m . Like $[\text{FeL1}(\text{Cl}_2)]^+$, the ferric iron adopted a *cis*-distorted octahedral geometry in which the equatorial plane was occupied by two nitrogen atoms of the macrocycle, a bridging oxide, and a chloride; the axial positions were filled by the two remaining nitrogen atoms in the macrocycle completing the coordination sphere. The asymmetric unit of **1a** consists of half of the molecule ($\text{O-FeL1}(\text{Cl})$) and two perchlorate counter-ions. The

complete complex is symmetry generated by a two-fold rotation about the oxygen atom, resulting in a 180° twist angle between the two pyridine moieties of the **L1** backbone. The Fe-O bond length, Fe(1)-O-Fe(1A) bond angle, and Fe...Fe distance (1.765(3) Å, 171(2)°, 3.592 Å, respectively) are consistent with previously reported μ -oxodiiron species containing chloride ligands.^{66, 71}

The prevalence of twinning in crystals of **1a** using slow evaporation of MeOH prompted us to investigate other crystal growth conditions. The slow diffusion of Et₂O into a solution of **1a** in CH₃CN afforded dark brown brick shaped crystals suitable for diffraction studies. The structure adopts the space group I4₁/a. The asymmetric unit consisted of the diiron(III) complex (**FeL1(Cl)-O-FeL1(Cl)**), a perchlorate counter-ion, a chloride counter-ion, and one molecule of CH₃CN. This was the first indication that the oxo-bridge dimer in **1** may exist with different geometries in the solid state. The orientation of the ligands with respect to one another was quantified by the twist angle between the pyridine moieties. The twist angle of **1b** was 35.53(4)°, a difference of 35° compared to **1a**. Otherwise, the Fe(1)-O bond length (1.775(4) Å), the Fe(2)-O bond length (1.782(4) Å), Fe(1)-O-Fe(2) bond angle (166.7(3)°), and the Fe...Fe distance (3.533 Å) are comparable to **1a**. The ability to isolate multiple solid-state species of **1** indicated that multiple configurations may be thermodynamically similar in energy and packing dependent on solvent. This is evidenced by hydrogen bonding with free chloride in **1b**.

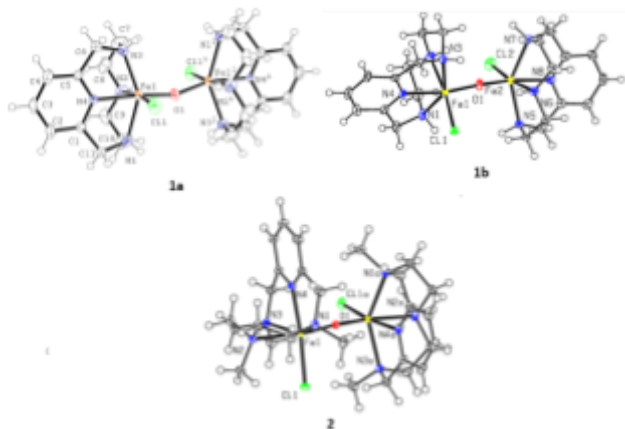


Figure 3. ORTEP (50% TELP) representation of solid-state structures of **1a**, **1b**, and **2**, described in Scheme 2. Counter ions and solvent molecules have been removed for clarity.

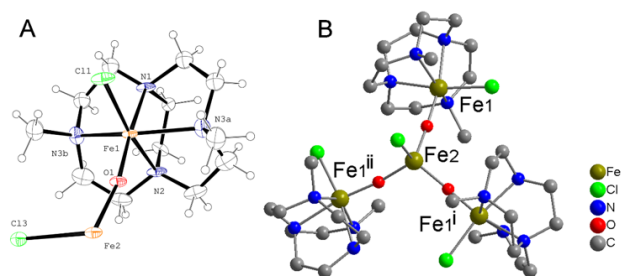


Figure 4. (A) ORTEP plot of the asymmetric unit of **3**. Atoms are shown as 30% probability ellipsoids. The PF₆⁻ anion is not included for clarity. (B) Tetranuclear cluster present in **[Fe(Cl){(μ-O)FeL5Cl}₃](PF₆)₂**. Anions and hydrogen atoms (on **A**) are not shown. Symmetry operations used to generate equivalent atoms: *i* = 2-*y*, 1+*x*-*y*, *z*; *ii* = 1-*x*+*y*, 2-*x*, *z*.

Crystals of **2** suitable for X-ray diffraction were obtained by slow diffusion of Et₂O into CH₃CN at room temperature. A 55% yield was achieved by isolation of the brown brick-shaped crystals. As shown in Figure 3, the complex crystallized in the space group C2/c with a *cis*-folded octahedral geometry. The *cis*-coordination sites of both ferric ions were filled by a μ -oxide and a chloride ligand. The asymmetric unit of **2** resembled that of **1a** rather than **1b**, and consisted of one half of the dimer, two PF₆ counter-ions, and one molecule of CH₃CN. The oxygen atom was positioned on a 2₁-screw axis resulting in a 90° twist angle between the pyridine moieties. The Fe(1)-O bond length (1.775(4) Å), Fe(2)-O bond length (1.782(4) Å), Fe(1)-O-Fe(2) bond angle (166.7(3)°), and Fe...Fe distance (3.592 Å) were consistent with those observed in **1a** and **1b**.

Slow evaporation of the reaction solution containing CH₃CN, Et₃N, H₂O, and **[FeL5(Cl)₂]⁺** resulted in red plate-shaped crystals of **3**. The solid-state structure, shown in Figure 4, indicated that **3** is tetranuclear cluster with threefold symmetry, **[Fe(Cl){(μ-O)FeL5Cl}₃](PF₆)₂**. A central tetrahedral Fe³⁺ ion that lies on a 3-fold axis is coordinated by a single chloride and by three oxide anions that bridge to further Fe³⁺ ions coordinated by chloride and **L5**. The charge of this cluster is balanced by PF₆⁻ anions. The structure determination was complicated by extensive disorder as the molecule lies on the mirror plane. Further details are given in the SI. The oxo-bridges are close to linear (Fe(1)-O(1)-Fe(2) angle is 168.6(5)°) and the bond lengths are in agreement with the other structures here (Fe(1)-O(1) is 1.763(8) Å and O(1)-Fe(2) is 1.820(8) Å).⁷²⁻⁷⁴

The higher catalytic efficiency of **[FeL5(Cl)₂]⁺**, reported previously, compared to **[FeL1(Cl)₂]⁺** and **[FeL4(Cl)₂]⁺** in combination with the instability of **[Fe(Cl){(μ-O)FeL5Cl}₃]²⁺** suggested that the active catalytic species does not involve an Fe-O-Fe type molecule.⁷⁰

¹H NMR analysis of **1a** and **2**

The stability and magnetic properties of **1a** and **2** in MeOH were studied using ¹H-NMR (Figure S1). Both complexes exhibit resonances between 0-40 ppm. The presence of paramagnetically shifted resonances indicated that the dimers are stable in MeOH because the monomeric congeners of **1** and **2** are not visible by NMR. Furthermore, the observation of resonances at 40 ppm are typical for antiferromagnetically coupled iron centers.⁵²

Absorbance analysis of **1a** and **2** in MeOH and CH₃CN

The absorption spectra of μ-oxodiiron(III) complexes have been shown to exhibit three types of transitions in the visible region: an allowed oxo-Fe charge transfer (LMCT) (300-400 nm), d-d transition and weak oxo-Fe LMCT (400-550 nm), and a forbidden oxo-Fe CT (550-700 nm).⁷⁵ The allowed oxo-Fe CT is believed to borrow intensity from the adjacent allowed LMCT of μ-oxodiiron(III) complexes such that the spin forbidden d-d and oxo-Fe CT are observed. This principle is explained fully in work by Norman *et al.*⁷⁶ The identity of the transitions were assigned based on the analysis of absorption spectra of a series of [Fe₂(TPA)₂O(L)](ClO₄)_n complexes; variations in the ligand field strength of L resulted in Fe-O-Fe bond angles ranging from 125° to 180°. The series of [Fe₂(TPA)₂O(L)₂](ClO₄)_n complexes exhibited a band at 490 nm indicating that this transition was not affected by the Fe-O-Fe angle or ligand field strength. Therefore, the transition was assigned as a spin-forbidden (⁴E and ⁴A₁) ← ⁶A₁, because the d⁵ Tanabe-Sugano diagram showed that the energy of two states, ⁴E and ⁴A₁, are independent of ligand field strength in high-spin complexes. This transition (490 nm) was assigned as a forbidden oxo-Fe CT because the absorbance bands between 550-700 nm varied with Fe-O-Fe angle and are accompanied by a low extinction coefficient. For linear μ-oxodiiron(III) complexes, absorbance bands at 550-580 nm are expected, corresponding to a d-d and oxo-Fe CT transition.^{68, 71, 76-77}

Solid-state analysis showed that the use of MeOH and CH₃CN for crystal growth resulted in two different complexes, **1a** (MeOH) and **1b** (CH₃CN). Therefore, the absorption spectrum of **1a** was obtained in MeOH and CH₃CN to validate the expected interconversion between **1a** and **1b** in solution. The absorbance maxima are available in Table S1 and the absorption spectra are shown in Figure 5 for MeOH and CH₃CN. When dissolved, the brown solution of **1a** exhibited absorption bands between 330 and 600 nm. The allowed oxo-Fe charge transfer band of **1a** was observed at 330 nm (3500 M⁻¹ cm⁻¹) in MeOH and 335 nm (10000 M⁻¹cm⁻¹) in CH₃CN. In MeOH, the absorbance band at 500 nm (170 M⁻¹, cm⁻¹) was consistent with a (⁴E and ⁴A₁) ← ⁶A₁ transition. However in CH₃CN, two absorption bands are observed (481 nm, ε = 932 M⁻¹, cm⁻¹; 500 nm ε = 878 M⁻¹,

cm⁻¹). The forbidden oxo-Fe CT was not observed in MeOH or CH₃CN.

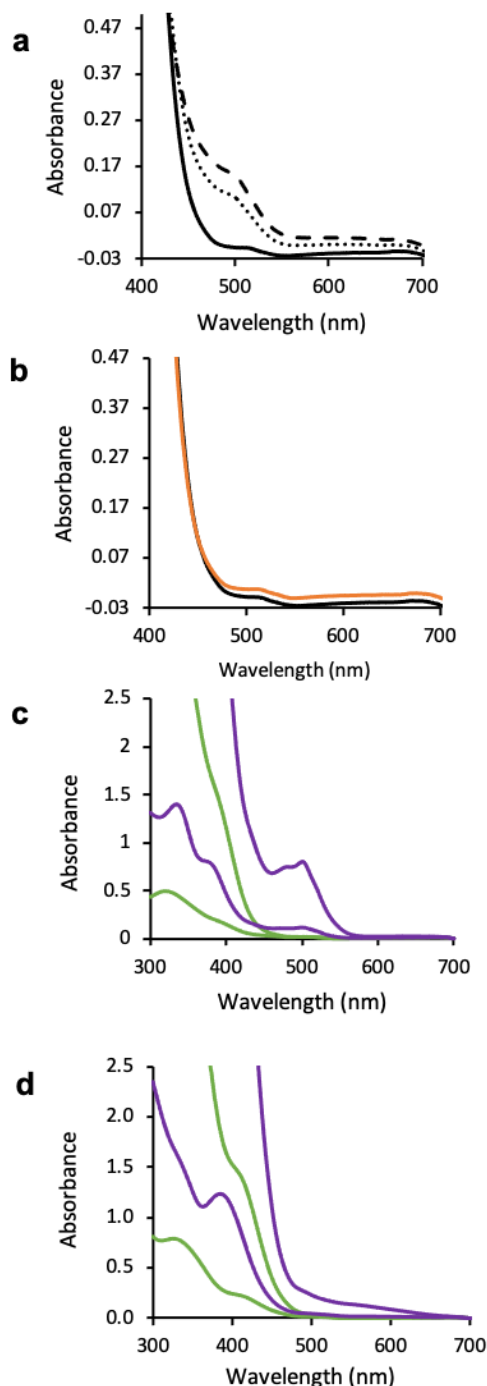


Figure 5. (a) Visible spectra of **1a** in MeOH (dashed-line), [FeL1(Cl)₂]⁺ in 8% H₂O/MeOH (dotted-line), and [FeL1(Cl)₂]⁺ in 8% H₂O/MeOH/25 μL acid (solid-line); (b) Visible absorption spectra of [FeL1(Cl)₂]⁺ in CH₃CN (orange) and 8% H₂O/MeOH solution after addition of concentrated HCl (25 μL, black). (c) [FeL1(Cl)₂]⁺ (0.13 mM/0.94 mM, green) and **1a** (0.13 mM/ 0.99 mM, purple); (d) [FeL4(Cl)₂]⁺ (0.16 mM/ 1.0 mM, green) and **2** (0.12 mM/1.0 mM, purple) in CH₃CN.

Attempts to compare spectra of $[\text{FeL1}(\text{Cl})_2]^+$ to **1a** in MeOH were limited by solubility. Therefore, an 8% $\text{H}_2\text{O}/\text{MeOH}$ solution was used to dissolve $[\text{FeL1}(\text{Cl})_2]^+$. An absorption band at 498 nm was observed, indicating that **1a** forms in the presence of H_2O as (Figure 4). The addition of 25 μL of concentrated HCl resulted in the disappearance of the band at 498 nm, confirming the existence of an equilibrium between **1a** and $[\text{FeL1}(\text{Cl})_2]^+$.

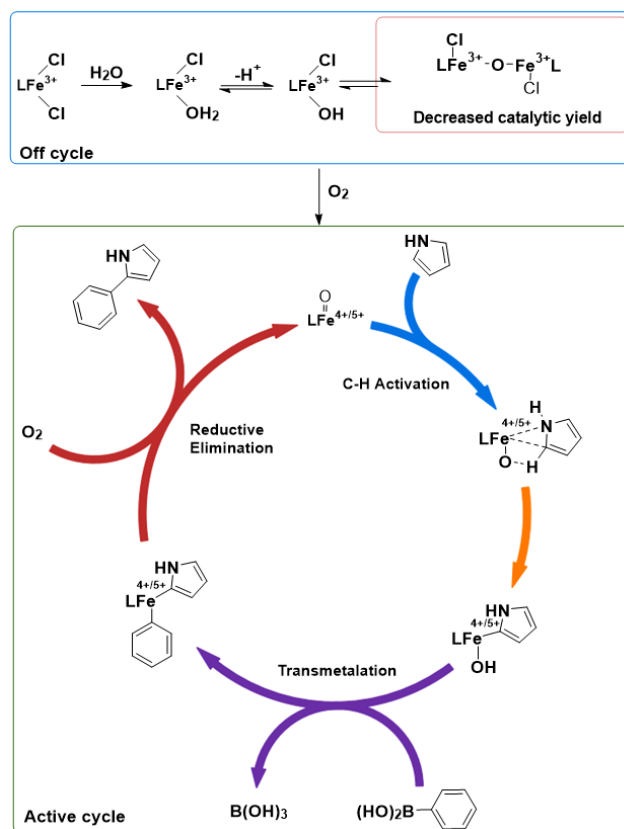
When dissolved in CH_3CN , solutions of $[\text{FeL1}(\text{Cl})_2]^+$ and $[\text{FeL4}(\text{Cl})_2]^+$ were pale yellow, while **1a** and **2** were brown. The absorbance data can be found in Figure 5 and Table S1. Two LMCT bands are observed: $[\text{FeL1}(\text{Cl})_2]^+$, at 319 nm ($4\,500\text{ M}^{-1}\text{cm}^{-1}$) and 390 nm (sh; $1\,600\text{ M}^{-1}\text{cm}^{-1}$); and $[\text{FeL4}(\text{Cl})_2]^+$, at 326 nm ($5\,000\text{ M}^{-1}\text{cm}^{-1}$) and 408 nm (sh; $1\,400\text{ M}^{-1}\text{cm}^{-1}$). No other absorption bands were observed for $[\text{FeL1}(\text{Cl})_2]^+$ and $[\text{FeL4}(\text{Cl})_2]^+$. Complexes **1a** and **2** exhibited four absorption bands between 300 and 700 nm, which are consistent with other μ -oxodiiron(III) complexes.^{71, 76-77} The formation of an Fe-O-Fe bridged complex greatly increased the extinction coefficient of bands between 300 – 410 nm. This is attributed to a two-fold increase in iron atom concentration in combination with the additive effect of the LMCT and the oxo-Fe CT transitions. The signature absorption bands at 490 nm and 550 nm, corresponding to the forbidden (${}^4\text{E}$ and ${}^4\text{A}_1$) \leftarrow ${}^6\text{A}_1$ and oxo-Fe CT respectively, are observed at 481 nm ($932\text{ M}^{-1}\text{cm}^{-1}$) and 500 nm ($878\text{ M}^{-1}\text{cm}^{-1}$) for **1a**, and 495 nm (sh; $51\text{ M}^{-1}\text{cm}^{-1}$) and 567 (sh; $161\text{ M}^{-1}\text{cm}^{-1}$) for **2**.

Dimerization of $[\text{FeL1}(\text{Cl})_2]^+$ in reaction conditions

Finally, the ability of pyrrole to promote formation of **1a** was tested. Interestingly, the addition of up to 4 equivalents of pyrrole had no effect on the absorption spectra of $[\text{FeL1}(\text{Cl})_2]^+$, but the addition of excess pyrrole, 200 μL (800 eq.), resulted in dimer formation based on the appearance of an absorption band at 498 nm upon pyrrole addition.

The conversion of monomeric iron complexes into μ -oxodiiron complexes may occur in the presence of excess water. Therefore, the large excess of pyrrole needed is most likely due to the low H_2O content in the pyrrole. These results indicate dimer formation can be promoted under coupling reaction conditions, due to the presence of H_2O in the pyrrole used, despite distillation for purification prior to use. In the catalytic cycle, complexes **1a** and **2** are assigned as off-cycle species. Therefore, the formation of **1a** and **2** may contribute to the decreased activity of $[\text{FeL1-L4}(\text{Cl})_2]^+$ compared to $[\text{FeL5}(\text{Cl})_2]^+$ in the coupling of pyrrole and phenylboronic acid.⁵⁴ In order to test this hypothesis, the coupling reaction was performed with the dimer **1a**. The observed yield of 2-phenylpyrrole was 28(8)%, which is significantly lower than the corresponding monomeric

species. This finding validates that the dimers are off cycle species that result in decreased catalytic yields.



Scheme 4. More detailed catalytic mechanism proposed for the iron-catalyzed C-C coupling of pyrrole and phenylboronic acid. Active cycle (outlined in green) based on ref.^{11, 17}

CONCLUSIONS

In conclusion, this work set out to address specific questions related to the mechanism of the iron catalyzed C-C coupling reaction. The results indicate that an oxidant is needed in the iron-catalyzed C-C coupling reaction of phenylboronic acid and pyrrole. Air and perchlorate are viable sacrificial oxidants; however, more experiments are needed to understand the true reactivity of perchlorate as a sacrificial oxidant. Oxidized pyrrole was tested and found unable to react with phenylboronic acid to produce 2-phenylpyrrole, thereby, implicating oxygen reacts with the iron center. Furthermore, the presence of radical scavengers in the form of complexes $[\text{FeL2}(\text{Cl})_2]^+$ and $[\text{FeL3}(\text{Cl})_2]^+$ did not decrease catalytic yields. This, combined with DFT studies and literature precedent, suggest a high valent Fe(IV) or Fe(V)-oxo species should be considered in addition to the other, low valent mechanisms proposed to date.^{13-14, 21} The monomeric iron complexes $[\text{FeL1}(\text{Cl})_2]^+$ and $[\text{FeL4}(\text{Cl})_2]^+$ readily form μ -oxodiiron species in the presence of a

base and H₂O. In the solid state, the more topologically constrained [FeL5(Cl)₂]⁺ does not form a dimeric complex, but a tetranuclear cluster with a (Cl)FeO₃ core, [Fe(Cl){(μ-O)FeL5(Cl)}₃]²⁺. Comparison of the absorption spectra of **1a** in CH₃CN to that of the monomer [FeL1(Cl)₂]⁺, after addition of pyrrole, indicates that **1a** can form during the coupling of pyrrole and phenylboronic acid. The μ-oxodiiron species (**1** and **2**) are assigned as off-cycle complexes that lower catalytic yield, as evidenced by the bona fide dimers resulting in significantly lower yields compared to monomers congeners.

The identification of dimer formation under coupling conditions, the need for oxygen, the inability of oxidized pyrrole to act as a starting material to produce 2-phenylpyrrole, and the fact that radical scavenging catalysts [FeL2(Cl)₂]⁺ and [FeL3(Cl)₂]⁺ give comparable yields to [FeL1(Cl)₂]⁺, have led to a more detailed mechanism, relative to the literature,¹¹⁻¹² shown in Scheme 4. Based on the radical studies reported above, we can postulate an Fe(IV)/Fe(V)-oxo derived mechanism. Attempts to characterize spectroscopically, or isolate a high valent species, were unsuccessful. Studies focused on isolating these intermediates from the reaction are precluded here due to the reaction being carried out in neat pyrrole, which polymerizes into dense poly-pyrrole, a well-known and unavoidable phenomenon. However, an acylperoxo-Fe(III) in equilibrium with an oxo-Fe^{IV} and Fe^V when [FeL4(OTf)₂] is exposed to oxidant.^{22, 78-79} To further support this, iron hydroxides form readily.⁸⁰ The Fe^{III}(OH) species of the L1-L3 complexes is likely present in pyrrole, based on speciation curves derived potentiometric studies⁸¹ that indicate this species is present at pH values >.8.5. The Fe^{III}(OH) species could readily oxidize to higher valent species, which is supported by our DFT and experiments by others.⁷⁸⁻⁷⁹ Therefore, due to the ambiguity of the oxidation states (Fe^{IV} vs Fe^V) within the active catalytic cycle, both possibilities are represented (Scheme 4). Notably though, the oxidation state of the Fe center after reductive elimination is not zero, which is observed in the case of Pd-catalyzed Suzuki-Miyaura coupling reactions.

Altogether, the studies presented here have resulted in experimental evidence to develop a more detailed catalytic mechanism for the coupling of pyrrole and phenylboronic acid in the presence of an iron(III) pre-catalyst. A helpful comment from a reviewer also noted that this reaction could also be considered complementary to C-H bond activation reported by Nakamura and Akkerman and the parallels are certainly striking.⁸²⁻⁸⁵ Such studies should be carefully considered when exploring the potential scope of this catalyst library.

EXPERIMENTAL SECTION

Pyrrole was distilled before use, all other reagents were obtained from commercial sources and used as

received, unless noted otherwise. NMR spectra were obtained on a 400-MHz Bruker Avance spectrometer, using deuterated solvents (MeOD or CDCl₃). NMR spectra were referenced using the corresponding solvent resonance (in parts per million; CDCl₃ δ = 7.26, MeOD δ = 3.31). Elemental analysis was performed by Canadian Microanalytical Service Ltd. Electronic absorption spectra were recorded on a Cary 60 UV-vis spectrophotometer using a 3 mL quartz cuvette with a 1 cm path length. Catalytic cycles were drawn using a recently reported web based interface.⁸⁶

X-ray diffraction analysis. Single crystal X-ray diffraction data were collected at 100 K on a Bruker D8 Quest Diffractometer. Data collection, frame integration, data reduction, absorption (multi-scan), and structure determination were carried out using APEX2 software. Structural refinements were performed with XShell (v 6.3.1), by the full-matrix least-squares method. All non-hydrogen atoms were refined using anisotropic thermal parameters, while the hydrogen atoms were treated as mixed. The ORTEP molecular plots (50 %) were produced using APEX2 (Version 2014.9-0).

[μ-O(FeL1Cl)₂](ClO₄)₂ (1a**):** Crystalline [FeL1(Cl)₂]ClO₄ (34.0 mg, 0.08 mmol) was dissolved in 1 mL water and diluted with 5 mL MeOH. Et₃N (10.9 μL, 0.0786 mmol) was dissolved in 600 μL of MeOH and added dropwise to [FeL1(Cl)₂]ClO₄. The solution was stirred for 1hr, followed by slow evaporation of solvent to afford black X-ray quality crystals over the course of several days. Yield: 50 % (32.0 mg, 0.04 mmol). Elemental analysis Calc (Found): C₂₂H₃₆Cl₄Fe₂N₈O₉; C 32.62 (32.22); H 4.48 (4.50); N 13.83 (13.70). CCDC # 1578765. Note: **1a** and **1b** (CCDC # 2018374) are different orientations of the same molecule, which we attribute to solvent used in crystal growth.

[μ-O(FeL4Cl)₂](PF₆)₂·CH₃CN (2**):** Complex [FeL4(Cl)₂]PF₆ (39.7 mg, 0.076 mmol) was dissolved in 12.5 μL water and 1 mL CH₃CN. Et₃N (16.17 μL, 0.116 mmol) was dissolved in 300 μL CH₃CN and added dropwise to [FeL4(Cl)₂]PF₆. The reaction was stirred for 1 h, then placed in Et₂O. Black X-ray quality crystals formed over the course of 6 h. Yield: 55.2% (22.8 mg, 0.021 mmol). Elemental analysis Calc (Found): C₃₀H₅₁N₈Fe₂Cl₂OP₂F₁₂; C 35.11 (35.50); H 5.01 (5.09); N 12.28 (12.81). CCDC # 1813235.

[Fe(Cl){(μ-O)FeL5(Cl)}₃](PF₆)₂ (3**)** was prepared in the same manner as (**2**). Lack of substantial product precluded successful characterization beyond X-ray diffraction. CCDC # 2013199.

2-phenylpyrrole yield determination: Phenylboronic acid (24 mg, 0.2 mmol) and crystalline material of the iron complex (0.02 mmol) were added to a 20 mL vial equipped with a stir bar. Degassed pyrrole (1 mL) was added to the flask, and the mixture was heated to 130°C for 10 h. The reaction was cooled to room temperature and the pyrrole was removed under vacuum until no visible liquid was present. Increasing the time that the reaction was kept under reduced pressure decreased yields. The product mixture was dissolved in a minimum amount of CDCl₃, and 5 μL of dimethyldiphenylsilane was added to the solution as a standard. The solution was filtered through a 0.2 μm nylon filter and a known amount of sample was added to a

pre-weighed NMR tube. Yield determinations were performed using three resonances: 6.875, 6.532, and 6.307 ppm, corresponding to 2-phenylpyrrole and a resonance at 0.533 ppm corresponding to dimethyldiphenylsilane. The reported values are averages of all resonances; each measurement was carried out in triplicate.

General coupling reactions in anaerobic conditions: Phenylboronic acid (24 mg, 0.20 mmol) and catalyst (0.02 mmol, 0.20 mmol), if used, were added to a 2 mL flask equipped with a stir bar, the system was then placed under an atmosphere of nitrogen. Pyrrole (1ml) was added to flask and the mixture was heated to 130°C for 10 h. An identical work-up to that described above was followed.

3-pyrroline-2-one coupling reactions: aerobic conditions Phenylboronic acid (24 mg, 0.20 mmol) and $[\text{FeL}(\text{Cl})_2]\text{ClO}_4$ (8 mg, 0.02 mmol) were added to a test tube equipped with a stir bar. 3-pyrroline-2-one (1 mL) was added to flask and the mixture was heated to 130 °C. After refluxing for 10 h, the reaction was cooled to room temperature, and the crude product was dried under reduced pressure until no visible liquid was present. NMR of the crude reaction showed no formation of 2-phenylpyrrole.

Anaerobic conditions: Phenylboronic acid (24 mg, 0.20 mmol) and $[\text{FeL}(\text{Cl})_2]\text{ClO}_4$ (8 mg, 0.02 mmol) were added to a 2 mL reaction vessel equipped with a stir bar, and the system was placed under an inert atmosphere using Schlenk techniques. 1 mL 3-pyrroline-2-one was added and the system was heated to 130°C for 10 h. Formation of 2-phenylpyrrole was not observed.

DPPH assay: A 2,2-diphenyl-1-picrylhydrazyl (DPPH) stock solution was made by dissolving 25 mg of DPPH in 100 mL of absolute EtOH. The solution was standardized to 1.32 absorbance units (0.137 mM) by dilution with absolute EtOH. 1 mg of each complex was dissolved in 2 mL of water to yield the following concentrations: 1.2 mM $[\text{FeL}(\text{Cl})_2]\text{ClO}_4$, 1.4 mM $[\text{FeL}(\text{Cl})_2]\text{ClO}_4$, 1.0 mM $[\text{FeL}(\text{Cl})_2]\text{ClO}_4$. The pH was adjusted with HCl gas to dissolve the compounds in water. 1 mg of BHT was dissolved in 2 mL of absolute EtOH to make a 2.3 mM stock solution of BHT. Each complex and BHT were diluted to reach the following concentrations: 0.75 mM, 0.5 mM, 0.25 mM, and 0.1 mM. 150 μL of each solution were put into a microplate well with 150 μL of 0.137 M DPPH. The solutions were incubated in the dark for 24 h, and the absorbance was measured at 515 nm. The experiment was done in

triplicate. A 50:50 mixture of EtOH and water served as the negative control. A mixture of 150 μL of H_2O and 150 μL of DPPH, as well as, a mixture of 150 μL of absolute EtOH and 150 μL of DPPH served as positive controls for the complexes and BHT respectively.

DFT Studies: Calculations use the Gaussian 16 package.⁸⁷ Calculations simulate isolated high-spin $[\text{Fe}^{\text{III}}\text{LCl}_2]^+$ and $[\text{Fe}^{\text{III}}\text{L}(\text{Cl})\text{OH}]^+$ complexes (charge +1, spin multiplicity 6) and the oxidation products $[\text{Fe}^{\text{IV}}\text{LCl}_2]^{2+}$ (charge +2, spin multiplicity 5) or $[\text{Fe}^{\text{IV}}(\text{=O})\text{LCl}]^+$ (charge +1, spin multiplicity 5) oxidation states. Complex geometries are optimized using density functional theory (DFT) with the B3LYP exchange-correlation functional⁸⁸⁻⁹⁰, the LANL2DZ⁹¹ basis set, and the SMD continuum model⁹² for water solvent. Calculations at these geometries are performed using the def2-TZVPP basis set⁹³⁻⁹⁴, SMD continuum water, and the B3LYP, Perdew-Burke-Ernzerhof (PBE) exchange-correlation⁹⁵, or M06-2X⁹⁶ exchange-correlation functionals. Values reported are total energies, Delta E. Partial atomic charges are computed using natural population analysis.⁹⁷

ASSOCIATED CONTENT

Supporting Information

The Supporting Information is available free of charge on the ACS Publications website and includes additional NMR, UV-vis, XRD, and DFT details.

AUTHOR INFORMATION

Corresponding Author kayla.green@tcu.edu

CONFLICTS OF INTEREST

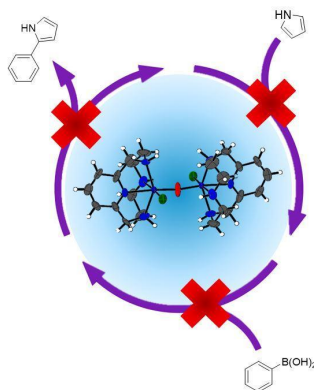
There are no conflicts to declare

ACKNOWLEDGMENT

The authors acknowledge National Institutes of Health R15GM123463 (to K.N.G.), Donors of the American Chemical Society Petroleum Research Fund (to T.J.H.), as well as the Henry Dreyfus Teacher-Scholar Awards Program (to T.J.H.) for support of this work

REFERENCES

1. Miyaura, N.; Suzuki, A., Stereoselective synthesis of arylated (E)-alkenes by the reaction of alk-1-enylboranes with aryl halides in the presence of palladium catalyst. *Journal of the Chemical*



- Society, Chemical Communications* **1979**, (19), 866-867.
2. Miyaura, N.; Yamada, K.; Suzuki, A., A new stereospecific cross-coupling by the palladium-catalyzed reaction of 1-alkenylboranes with 1-alkenyl or

- 1-alkynyl halides. *Tetrahedron Letters* **1979**, *20* (36), 3437-3440.
- Wu, G.; Jacobi von Wangelin, A., Iron-catalysed Suzuki biaryl couplings. *Nature Catalysis* **2018**, *1* (6), 377-378.
 - Shang, R.; Ilies, L.; Nakamura, E., Iron-Catalyzed C–H Bond Activation. *Chemical Reviews* **2017**, *117* (13), 9086-9139.
 - Andrews, N. C., Disorders of Iron Metabolism. *New England Journal of Medicine* **1999**, *341* (26), 1986-1995.
 - Feig, A. L.; Lippard, S. J., Reactions of Non-Heme Iron(II) Centers with Dioxygen in Biology and Chemistry. *Chemical Reviews* **1994**, *94* (3), 759-805.
 - Nakamura, E.; Sato, K., Managing the scarcity of chemical elements. *Nature Materials* **2011**, *10* (3), 158-161.
 - Egorova, K. S.; Ananikov, V. P., Toxicity of Metal Compounds: Knowledge and Myths. *Organometallics* **2017**, *36* (21), 4071-4090.
 - Berger, O.; Winters, K. R.; Sabourin, A.; Dzyuba, S. V.; Montchamp, J.-L., On the cost of academic methodologies. *Organic Chemistry Frontiers* **2019**, *6* (12), 2095-2108.
 - Yang, Y.; Reber, A. C.; Gilliland, S. E.; Castano, C. E.; Gupton, B. F.; Khanna, S. N., Donor/Acceptor Concepts for Developing Efficient Suzuki Cross-Coupling Catalysts Using Graphene-Supported Ni, Cu, Fe, Pd, and Bimetallic Pd/Ni Clusters. *The Journal of Physical Chemistry C* **2018**, *122* (44), 25396-25403.
 - Wen, J.; Qin, S.; Ma, L. F.; Dong, L.; Zhang, J.; Liu, S. S.; Duan, Y. S.; Chen, S. Y.; Hu, C. W.; Yu, X. Q., Iron-mediated direct Suzuki-Miyaura reaction: a new method for the ortho-arylation of pyrrole and pyridine. *Org. Lett.* **2010**, *12* (12), 2694-7.
 - Dong, L.; Wen, J.; Qin, S.; Yang, N.; Yang, H.; Su, Z.; Yu, X.; Hu, C., Iron-Catalyzed Direct Suzuki–Miyaura Reaction: Theoretical and Experimental Studies on the Mechanism and the Regioselectivity. *ACS Catalysis* **2012**, *2* (8), 1829-1837.
 - Brewer, S. M.; Palacios, P. M.; Johnston, H. M.; Pierce, B. S.; Green, K. N., Isolation and identification of the pre-catalyst in iron-catalyzed direct arylation of pyrrole with phenylboronic acid. *Inorganica Chimica Acta* **2018**, *478*, 139-147.
 - Howard, J. K.; Rihak, K. J.; Bissember, A. C.; Smith, J. A., The Oxidation of Pyrrole. *Chemistry – An Asian Journal* **2016**, *11* (2), 155-167.
 - Sun, Y.; Tang, H.; Chen, K.; Hu, L.; Yao, J.; Shaik, S.; Chen, H., Two-State Reactivity in Low-Valent Iron-Mediated C–H Activation and the Implications for Other First-Row Transition Metals. *J. Am. Chem. Soc.* **2016**, *138* (11), 3715-3730.
 - Boddie, T. E.; Carpenter, S. H.; Baker, T. M.; DeMuth, J. C.; Cera, G.; Brennessel, W. W.; Ackermann, L.; Neidig, M. L., Identification and Reactivity of Cyclometalated Iron(II) Intermediates in Triazole-Directed Iron-Catalyzed C–H Activation. *J. Am. Chem. Soc.* **2019**, *141* (31), 12338-12345.
 - Dong, L.; Wen, J.; Qin, S.; Yang, N.; Yang, H.; Su, Z.; Yu, X.; Hu, C., Iron-Catalyzed Direct Suzuki-Miyaura Reaction: Theoretical and Experimental Studies on the Mechanism and the Regioselectivity. *ACS Catal.* **2012**, *2* (8), 1829-1837.
 - Choudhury, A. R.; Mukherjee, S., Organocatalytic asymmetric direct vinylogous Michael addition of [small alpha],[small beta]-unsaturated [gamma]-butyrolactam to nitroolefins. *Org. Biomol. Chem.* **2012**, *10* (36), 7313-7320.
 - Gamba, I.; Codolà, Z.; Lloret-Fillol, J.; Costas, M., Making and breaking of the OO bond at iron complexes. *Coord. Chem. Rev.* **2017**, *334*, 2-24.
 - McDonald, A. R.; Que, L., High-valent nonheme iron-oxo complexes: Synthesis, structure, and spectroscopy. *Coord. Chem. Rev.* **2013**, *257* (2), 414-428.
 - Fan, R.; Serrano-Plana, J.; Oloo, W. N.; Draksharapu, A.; Delgado-Pinar, E.; Company, A.; Martín-Diaconescu, V.; Borrell, M.; Lloret-Fillol, J.; García-España, E.; Guo, Y.; Bominaar, E. L.; Que, L.; Costas, M.; Münck, E., Spectroscopic and DFT Characterization of a

- Highly Reactive Nonheme FeV–Oxo Intermediate. *J. Am. Chem. Soc.* **2018**, *140* (11), 3916-3928.
22. Dantignana, V.; Serrano-Plana, J.; Draksharapu, A.; Magallón, C.; Banerjee, S.; Fan, R.; Gamba, I.; Guo, Y.; Que, L.; Costas, M.; Company, A., Spectroscopic and Reactivity Comparisons between Nonheme Oxoiron(IV) and Oxoiron(V) Species Bearing the Same Ancillary Ligand. *J. Am. Chem. Soc.* **2019**, *141* (38), 15078-15091.
 23. Lincoln, K. M.; Offutt, M. E.; Hayden, T. D.; Saunders, R. E.; Green, K. N., Structural, Spectral, and Electrochemical Properties of Nickel(II), Copper(II), and Zinc(II) Complexes Containing 12-Membered Pyridine- and Pyridol-Based Tetra-aza Macrocycles. *Inorg. Chem.* **2014**, *53* (3), 1406-1416.
 24. Patel, R.; Patel, N., In vitro antioxidant activity of coumarin compounds by DPPH, Super oxide and nitric oxide free radical scavenging methods. *Journal of Advanced Pharmacy Education & Research* **2011**, *1*, 52-68.
 25. Thaipong, K.; Boonprakob, U.; Crosby, K.; Cisneros-Zevallos, L.; Byrne, D. H., Comparison of ABTS, DPPH, FRAP, and ORAC assays for estimating antioxidant activity from guava fruit extracts. *Journal of Food Composition and Analysis* **2006**, *19* (6-7), 669-675.
 26. Mensor, L. L.; Menezes, F. S.; Leitao, G. G.; Reis, A. S.; dos Santos, T. C.; Coube, C. S.; Leitao, S. G., Screening of Brazilian plant extracts for antioxidant activity by the use of DPPH free radical method. *Phytotherapy Research* **2001**, *15* (2), 127-130.
 27. Lincoln, K. M.; Gonzalez, P.; Richardson, T. E.; Rutter, L.; Julovich, D. A.; Simpkins, J. W.; Green, K. N., A potent antioxidant small molecule aimed at targeting metal-based oxidative stress in neurodegenerative disorders. *Chem. Commun.* **2013**, *49*, 2712-2714.
 28. Lincoln, K. M.; Richardson, T. E.; Rutter, L.; Gonzalez, P.; Simpkins, J. W.; Green, K. N., An N-heterocyclic amine chelate capable of antioxidant capacity and amyloid disaggregation. *ACS Chem. Neurosci.* **2012**, *3* (11), 919-27.
 29. Steenken, S.; Oneill, P., Reaction of Oh Radicals with 2-Pyridones and 4-Pyridones in Aqueous-Solution - Electron-Spin Resonance and Pulse-Radiolysis Study. *J Phys Chem-US* **1979**, *83* (18), 2407-2412.
 30. Balamurugan, M.; Suresh, E.; Palaniandavar, M., Non-heme mu-Oxo- and bis(mu-carboxylato)-bridged diiron(III) complexes of a 3N ligand as catalysts for alkane hydroxylation: stereoelectronic factors of carboxylate bridges determine the catalytic efficiency. *Dalton Transactions* **2016**, *45* (28), 11422-11436.
 31. Balogh-Hergovich, E.; Speier, G.; Reglier, M.; Giorgi, M.; Kuzmann, E.; Vertes, A., Synthesis, structure, and catalytic activity of new mu-oxo-bridged diiron(III) complexes. *European Journal of Inorganic Chemistry* **2003**, (9), 1735-1740.
 32. Baranwal, B. P.; Das, S. S.; Gupta, T.; Singh, A. K., Novel trinuclear, oxo-bridged materials of mixed-valence iron with fatty acids. *Progress in Crystal Growth and Characterization of Materials* **2002**, *45* (1-2), 147-153.
 33. Bhattacharyya, J.; Das, S.; Mukhopadhyay, S., Mechanistic studies on oxidation of L-ascorbic acid by an oxo-bridged diiron complex in aqueous acidic media. *Dalton Transactions* **2007**, (12), 1214-1220.
 34. Bhattacharyya, J.; Mukhopadhyay, S., Mechanistic studies on the oxidation of hydroquinone by an oxo-bridged diiron(III,III) complex in weakly acidic aqueous media. *Transition Metal Chemistry* **2006**, *31* (2), 256-261.
 35. Chaudhuri, B.; Banerjee, R., Kinetics and mechanism of hydroxylamine oxidation by Fe-2(III)(mu-O)(phen)(4)(H2O)(2) (4+) in aqueous media. *Canadian Journal of Chemistry-Revue Canadienne De Chimie* **1998**, *76* (3), 350-355.
 36. Comba, P.; Gahan, L. R.; Hanson, G. R.; Mereacre, V.; Noble, C. J.; Powell, A. K.; Prisecaru, I.; Schenk, G.; Zajaczkowski-Fischer, M., Monoesterase Activity of a Purple Acid Phosphatase Mimic with a Cyclam Platform.

- Chemistry-a European Journal* **2012**, *18* (6), 1700-1710.
37. Cranswick, M. A.; Meier, K. K.; Shan, X.; Stubna, A.; Kaizer, J.; Mehn, M. P.; Muenck, E.; Que, L., Jr., Protonation of a Peroxodiiron(III) Complex and Conversion to a Diiron(III/IV) Intermediate: Implications for Proton-Assisted O-O Bond Cleavage in Nonheme Diiron Enzymes. *Inorganic Chemistry* **2012**, *51* (19), 10417-10426.
38. Das, S.; Bhattacharyya, J.; Mukhopadhyay, S., Mechanistic studies on oxidation of hydrogen peroxide by an oxo-bridged diiron complex in aqueous acidic media. *Dalton Transactions* **2008**, (46), 6634-6640.
39. Friedle, S.; Kodanko, J. J.; Morys, A. J.; Hayashi, T.; Moenne-Loccoz, P.; Lippard, S. J., Modeling the Syn Disposition of Nitrogen Donors in Non-Heme Diiron Enzymes. Synthesis, Characterization, and Hydrogen Peroxide Reactivity of Diiron(III) Complexes with the Syn N-Donor Ligand H(2)BPG(2)DEV. *Journal of the American Chemical Society* **2009**, *131* (40), 14508-14520.
40. Hazell, A.; Jensen, K. B.; McKenzie, C. J.; Toftlund, H., SYNTHESIS AND REACTIVITY OF (MU-OXO)DIIRON(III) COMPLEXES OF TRIS(2-PYRIDYLMETHYL)AMINE - X-RAY CRYSTAL-STRUCTURES OF TPA(OH)FEOFE(H₂O)TPA (CLO₄)₃ AND TPA(CL)FEOFE(CL)TPA (CLO₄)₂. *Inorganic Chemistry* **1994**, *33* (14), 3127-3134.
41. Ito, S.; Okuno, T.; Itoh, H.; Ohba, S.; Matsushima, H.; Tokii, T.; Nishida, Y., Chemical basis for high activity in oxygenation of cyclohexane catalyzed by dinuclear iron(III) complexes with ethereal oxygen containing ligand and hydrogen peroxide system. *Zeitschrift Fur Naturforschung Section B-a Journal of Chemical Sciences* **1997**, *52* (6), 719-727.
42. Ito, S.; Okuno, T.; Matsushima, H.; Tokii, T.; Nishida, Y., Chemical origin of high activity in oxygenation of cyclohexane by H₂O₂ catalysed by dinuclear iron(III) complexes with amide-containing ligands. *J Chem Soc Dalton* **1996**, (23), 4479-4484.
43. Ito, S.; Sasaki, Y.; Takahashi, Y.; Ohba, S.; Nishida, Y., Oxygenation of nucleosides by peroxide adduct of binuclear iron(III) complex with a mu-oxo bridge. *Zeitschrift Fur Naturforschung C-a Journal of Biosciences* **1999**, *54* (7-8), 554-561.
44. Jozwiuk, A.; Ingram, A. L.; Powell, D. R.; Mobaraki, B.; Chilton, N. F.; Murray, K. S.; Houser, R. P., Redox and acid-base properties of asymmetric non-heme (hydr)oxo-bridged diiron complexes. *Dalton Transactions* **2014**, *43* (25), 9740-9753.
45. Kejriwal, A.; Bandyopadhyay, P.; Biswas, A. N., Aromatic hydroxylation using an oxo-bridged diiron(III) complex: a bio-inspired functional model of toluene monooxygenases. *Dalton Transactions* **2015**, *44* (39), 17261-17267.
46. Kejriwal, A.; Biswas, A. N.; Choudhury, A.; Bandyopadhyay, P., Diferric oxo-bridged complexes of a polydentate aminopyridyl ligand: synthesis, structure and catalytic reactivity. *Transition Metal Chemistry* **2014**, *39* (8), 909-915.
47. Kejriwal, A.; Biswas, S.; Biswas, A. N.; Bandyopadhyay, P., cis-Dihydroxylation of electron deficient olefins oxo-bridged diiron(III) complex with H₂O₂. *Journal of Molecular Catalysis a-Chemical* **2016**, *413*, 77-84.
48. Kumbhar, A. S.; Damle, S. G.; Dasgupta, S. T.; Rane, S. Y.; Kumbhar, A. S., Nuclease activity of oxo-bridged diiron complexes. *Journal of Chemical Research* **1999**, (2), 98-99.
49. Liu, C. L.; Yu, S. W.; Li, D. F.; Liao, Z. R.; Sun, X. H.; Xu, H. B., DNA hydrolytic cleavage by the diiron(III) complex Fe-2(DTPB)(mu-O(mu-Ac)Cl)(BF₄)(2): Comparison with other binuclear transition metal complexes. *Inorganic Chemistry* **2002**, *41* (4), 913-922.
50. Mandal, P. C.; Bhattacharyya, J.; Das, S.; Mukhopadhyay, S.; Kirschenbaum, L. J., Mechanistic studies on the oxidation of pyruvic acid by an oxo-bridged diiron(III,III) complex in aqueous acidic media. *Polyhedron* **2009**, *28* (14), 3162-3168.

51. Mayilmurugan, R.; Stoeckli-Evans, H.; Suresh, E.; Palaniandavar, M., Chemoselective and biomimetic hydroxylation of hydrocarbons by non-heme mu-oxo-bridged diiron(III) catalysts using m-CPBA as oxidant. *Dalton Transactions* **2009**, (26), 5101-5114.
52. Menage, S.; Vincent, J. M.; Lambeaux, C.; Chottard, G.; Grand, A.; Fontecave, M., ALKANE OXIDATION CATALYZED BY MU-OXO-BRIDGED DIFFERIC COMPLEXES - A STRUCTURE-REACTIVITY CORRELATION STUDY. *Inorganic Chemistry* **1993**, 32 (22), 4766-4773.
53. Menage, S.; Vincent, J. M.; Lambeaux, C.; Fontecave, M., MU-OXO-BRIDGED DIIRON(III) COMPLEXES AND H₂O₂ - MONOOXYGENASE-LIKE AND CATALASE-LIKE ACTIVITIES. *J Chem Soc Dalton* **1994**, (14), 2081-2084.
54. Menage, S.; Vincent, J. M.; Lambeaux, C.; Fontecave, M., Alkane oxidation catalyzed by mu-oxo bridged diferric complexes: An overall mechanism. *Journal of Molecular Catalysis a-Chemical* **1996**, 113 (1-2), 61-75.
55. Nayak, S.; Dash, A. C., Kinetics and mechanism of the formation of (1,8)bis(2-hydroxybenzamido)3,6-diazaoctaneiron(III) and its reactions with thiocyanate, azide, acetate, sulfur(IV) and ascorbic acid in solution, and the synthesis and characterization of a novel oxo bridged diiron(III) complex. The role of phenol-amide-amine coordination. *Transition Metal Chemistry* **2006**, 31 (6), 813-828.
56. Okuno, T.; Ito, S.; Ohba, S.; Nishida, Y., mu-Oxo bridged diiron(III) complexes and hydrogen peroxide: oxygenation and catalase-like activities. *J Chem Soc Dalton* **1997**, (19), 3547-3551.
57. Pardo, E.; Lloret, F.; Carrasco, R.; Munoz, M. C.; Temporal-Sanchez, T.; Ruiz-Garcia, R., Chemistry and reactivity of dinuclear iron oxamate complexes: alkane oxidation with hydrogen peroxide catalysed by an oxo-bridged diiron(III) complex with amide and carboxylate ligation. *Inorganica Chimica Acta* **2004**, 357 (9), 2713-2720.
58. Payra, P.; Hung, S. C.; Kwok, W. H.; Johnston, D.; Gallucci, J.; Chan, M. K., Structural, magnetic and catalytic properties of a self-recognized mu-oxo-bridged diiron(III) bis(benzimidazole) complex. *Inorganic Chemistry* **2001**, 40 (16), 4036-4039.
59. Roy, M.; Bhowmick, T.; Santhanagopal, R.; Ramakumar, S.; Chakravarty, A. R., Photo-induced double-strand DNA and site-specific protein cleavage activity of L-histidine (mu-oxo)diiron(III) complexes of heterocyclic bases. *Dalton Transactions* **2009**, (24), 4671-4682.
60. Shan, X. P.; Que, L., High-valent nonheme iron-oxo species in biomimetic oxidations. *Journal of Inorganic Biochemistry* **2006**, 100 (4), 421-433.
61. Taktak, S.; Kryatov, S. V.; Haas, T. E.; Rybak-Akimova, E. V., Diiron(III) oxo-bridged complexes with BPMEN and additional monodentate or bidentate ligands: Synthesis and reactivity in olefin epoxidation with H₂O₂. *Journal of Molecular Catalysis a-Chemical* **2006**, 259 (1-2), 24-34.
62. Tanase, S.; Foltz, C.; de Gelder, R.; Hage, R.; Bouwman, E.; Reedijk, J., Control of the catalytic oxidations mediated by an oxo-bridged non-heme diiron complex: role of additives and reaction conditions. *Journal of Molecular Catalysis a-Chemical* **2005**, 225 (2), 161-167.
63. Visvaganesan, K.; Suresh, E.; Palaniandavar, M., Highly selective hydroxylation of alkanes catalyzed by (mu-oxo)bis(mu-carboxylato)-bridged diiron(III) complexes: involvement of mononuclear iron(III) species in catalysis. *Dalton Transactions* **2009**, (19), 3814-3823.
64. Wang, J.; Jian, F.; Zhuang, R.; Qiao, Y., A New mu-Oxo Dimer Iron(III) Complex: Synthesis, Characterization, and Electrocatalysis. *Synthesis and Reactivity in Inorganic Metal-Organic and Nano-Metal Chemistry* **2012**, 42 (5), 711-715.
65. Wasser, I. M.; Fry, H. C.; Hoertz, P. G.; Meyer, G. J.; Karlin, K. D., Photochemical organic oxidations and dechlorinations with a

- mu-oxo bridged heme/non-heme diiron complex. *Inorganic Chemistry* **2004**, *43* (26), 8272-8281.
66. Fleischer, E. B.; Srivastava, T. S., Structure and properties of mu-oxobis(tetraphenylporphineiron(III)). *Journal of the American Chemical Society* **1969**, *91* (9), 2403-2405.
67. Shakya, R.; Powell, D. R.; Houser, R. P., Unsupported μ -Oxo- and μ -Hydroxo-Iron(III) Dimers and Mononuclear Iron(III) Complexes with Pyridylbis(aminophenol) Ligands. *European Journal of Inorganic Chemistry* **2009**, *2009* (35), 5319-5327.
68. Kurtz, D. M., Oxo- and hydroxo-bridged diiron complexes: a chemical perspective on a biological unit. *Chem. Rev.* **1990**, *90* (4), 585-606.
69. McClain II, J. M.; Maples, D. L.; Maples, R. D.; Matz, D. L.; Harris, S. M.; Nelson, A. D. L.; Silversides, J. D.; Archibald, S. J.; Hubin, T. J., Dichloro(4,10-dimethyl-1,4,7,10-tetraazabicyclo[5.5.2]tetradecane)iron(III) hexafluorophosphate. *Acta Crystallographica Section C* **2006**, *62* (11), m553-m555.
70. Brewer, S. M.; Wilson, K. R.; Jones, D. G.; Reinheimer, E. W.; Archibald, S. J.; Prior, T. J.; Ayala, M. A.; Foster, A. L.; Hubin, T. J.; Green, K. N., Increase of Direct C–C Coupling Reaction Yield by Identifying Structural and Electronic Properties of High-Spin Iron Tetra-azamacrocyclic Complexes. *Inorg. Chem.* **2018**, *57* (15), 8890-8902.
71. Hazell, A.; Jensen, K. B.; McKenzie, C. J.; Toftlund, H., Synthesis and Reactivity of (μ -Oxo)diiron(III) Complexes of Tris(2-pyridylmethyl)amine. X-ray Crystal Structures of [tpa(OH)FeOFe(H₂O)tpa](ClO₄)₃ and [tpa(Cl)FeOFe(Cl)tpa](ClO₄)₂. *Inorganic Chemistry* **1994**, *33* (14), 3127-3134.
72. Chanda, A.; Popescu, D.-L.; de Oliveira, F. T.; Bominaar, E. L.; Ryabov, A. D.; Münck, E.; Collins, T. J., High-valent iron complexes with tetraamido macrocyclic ligands: Structures, Mössbauer spectroscopy, and DFT calculations. *Journal of Inorganic Biochemistry* **2006**, *100* (4), 606-619.
73. Bigelow, J. O.; England, J.; Klein, J. E. M. N.; Farquhar, E. R.; Frisch, J. R.; Martinho, M.; Mandal, D.; Münck, E.; Shaik, S.; Que, L., Oxoiron(IV) Tetramethylcyclam Complexes with Axial Carboxylate Ligands: Effect of Tethering the Carboxylate on Reactivity. *Inorg. Chem.* **2017**, *56* (6), 3287-3301.
74. England, J.; Guo, Y.; Farquhar, E. R.; Young Jr, V. G.; Münck, E.; Que Jr, L., The Crystal Structure of a High-Spin Oxoiron(IV) Complex and Characterization of Its Self-Decay Pathway. *J. Am. Chem. Soc.* **2010**, *132* (25), 8635-8644.
75. Kurtz, D. M., Oxo-bridged and hydroxo-bridged diiron complexes - A chemical perspective on a biological unit. *Chemical Reviews* **1990**, *90* (4), 585-606.
76. Norman, R. E.; Holz, R. C.; Menage, S.; Que, L.; Zhang, J. H.; O'Connor, C. J., Structures and properties of dibridged (μ -oxo)diiron(III) complexes. Effects of the Fe-O-Fe angle. *Inorganic Chemistry* **1990**, *29* (23), 4629-4637.
77. Menage, S.; Vincent, J. M.; Lambeaux, C.; Chottard, G.; Grand, A.; Fontecave, M., Alkane oxidation catalyzed by μ -oxo-bridged diferric complexes: a structure/reactivity correlation study. *Inorganic Chemistry* **1993**, *32*, 4766-4773
78. Serrano-Plana, J.; Oloo, W. N.; Acosta-Rueda, L.; Meier, K. K.; Verdejo, B.; García-España, E.; Basallote, M. G.; Münck, E.; Que, L.; Company, A.; Costas, M., Trapping a Highly Reactive Nonheme Iron Intermediate That Oxygenates Strong C—H Bonds with Stereoretention. *J. Am. Chem. Soc.* **2015**, *137* (50), 15833-15842.
79. Fan, R.; Serrano-Plana, J.; Oloo, W. N.; Draksharapu, A.; Delgado-Pinar, E.; Company, A.; Martin-Diaconescu, V.; Borrell, M.; Lloret-Fillol, J.; Garcia-Espana, E.; Guo, Y.; Bominaar, E. L.; Que, L., Jr.; Costas, M.; Munck, E., Spectroscopic and DFT Characterization of a Highly Reactive Nonheme Fe(V)-Oxo Intermediate. *J. Am. Chem. Soc.* **2018**, *140* (11), 3916-3928.

80. Brown, P. L.; Ekberg, C., *Hydrolysis of metal ions*. John Wiley & Sons: 2016.
81. Mekhail, M. A.; Pota, K.; Schwartz, T. M.; Green, K. N., Functionalized pyridine in pyclen-based iron (iii) complexes: evaluation of fundamental properties. *RSC Advances* **2020**, *10* (52), 31165-31170.
82. Ilies, L.; Matsubara, T.; Ichikawa, S.; Asako, S.; Nakamura, E., Iron-catalyzed directed alkylation of aromatic and olefinic carboxamides with primary and secondary alkyl tosylates, mesylates, and halides. *J. Am. Chem. Soc.* **2014**, *136* (38), 13126-13129.
83. Norinder, J.; Matsumoto, A.; Yoshikai, N.; Nakamura, E., Iron-Catalyzed Direct Arylation through Directed C–H Bond Activation. *J. Am. Chem. Soc.* **2008**, *130* (18), 5858-5859.
84. Gu, Q.; Al Mamari, H. H.; Graczyk, K.; Diers, E.; Ackermann, L., Iron-Catalyzed C (sp²)–H and C (sp³)–H Arylation by Triazole Assistance. *Angew. Chem.* **2014**, *53* (15), 3868-3871.
85. Cera, G.; Haven, T.; Ackermann, L., Expedient Iron-Catalyzed C–H Allylation/Alkylation by Triazole Assistance with Ample Scope. *Angewandte Chemie* **2016**, *128* (4), 1506-1510.
86. McFarlane, J.; Henderson, B.; Donnecke, S.; McIndoe, J. S., An Information-Rich Graphical Representation of Catalytic Cycles. *Organometallics* **2019**, *38* (21), 4051-4053.
87. Frisch, M. J.; Trucks, G. W.; Schlegel, H. B.; Scuseria, G. E.; Robb, M. A.; Cheeseman, J. R.; Scalmani, G.; Barone, V.; Petersson, G. A.; Nakatsuji, H.; Li, X.; Caricato, M.; Marenich, A. V.; Bloino, J.; Janesko, B. G.; Gomperts, R.; Mennucci, B.; Hratchian, H. P.; Ortiz, J. V.; Izmaylov, A. F.; Sonnenberg, J. L.; Williams; Ding, F.; Lipparini, F.; Egidi, F.; Goings, J.; Peng, B.; Petrone, A.; Henderson, T.; Ranasinghe, D.; Zakrzewski, V. G.; Gao, J.; Rega, N.; Zheng, G.; Liang, W.; Hada, M.; Ehara, M.; Toyota, K.; Fukuda, R.; Hasegawa, J.; Ishida, M.; Nakajima, T.; Honda, Y.; Kitao, O.; Nakai, H.; Vreven, T.; Throssell, K.; Montgomery Jr., J. A.; Peralta, J. E.; Ogliaro, F.; Bearpark, M. J.; Heyd, J. J.; Brothers, E. N.; Kudin, K. N.; Staroverov, V. N.; Keith, T. A.; Kobayashi, R.; Normand, J.; Raghavachari, K.; Rendell, A. P.; Burant, J. C.; Iyengar, S. S.; Tomasi, J.; Cossi, M.; Millam, J. M.; Klene, M.; Adamo, C.; Cammi, R.; Ochterski, J. W.; Martin, R. L.; Morokuma, K.; Farkas, O.; Foresman, J. B.; Fox, D. J. *Gaussian 16 Rev. C.01*, Wallingford, CT, 2016.
88. Becke, A. D., A new mixing of Hartree–Fock and local density-functional theories. *The Journal of chemical physics* **1993**, *98* (2), 1372-1377.
89. Becke, A. D., Density-Functional Thermochemistry .3. The Role of Exact Exchange. *Journal of Chemical Physics* **1993**, *98* (7), 5648-5652.
90. Stephens, P. J.; Devlin, F. J.; Chabalowski, C. F.; Frisch, M. J., Ab initio calculation of vibrational absorption and circular dichroism spectra using density functional force fields. *The Journal of physical chemistry* **1994**, *98* (45), 11623-11627.
91. Hay, P. J.; Wadt, W. R., Ab initio effective core potentials for molecular calculations. Potentials for the transition metal atoms Sc to Hg. *The Journal of chemical physics* **1985**, *82* (1), 270-283.
92. Marenich, A. V.; Cramer, C. J.; Truhlar, D. G., Universal solvation model based on solute electron density and on a continuum model of the solvent defined by the bulk dielectric constant and atomic surface tensions. *The Journal of Physical Chemistry B* **2009**, *113* (18), 6378-6396.
93. Andrae, D.; Haeussermann, U.; Dolg, M.; Stoll, H.; Preuss, H., Energy-adjusted ab initio pseudopotentials for the second and third row transition elements. *Theoretica chimica acta* **1990**, *77* (2), 123-141.
94. Weigend, F.; Ahlrichs, R., Balanced basis sets of split valence, triple zeta valence and quadruple zeta valence quality for H to Rn: Design and assessment of accuracy. *Phys Chem Chem Phys* **2005**, *7* (18), 3297-3305.
95. Perdew, J. P.; Burke, K.; Ernzerhof, M., Generalized gradient approximation made

- simple. *Physical review letters* **1996**, 77 (18), 3865.
96. Zhao, Y.; Truhlar, D. G., The M06 suite of density functionals for main group thermochemistry, thermochemical kinetics, noncovalent interactions, excited states, and transition elements: two new functionals and systematic testing of four M06-class functionals and 12 other functionals. *Theor Chem Acc* **2008**, 120 (1), 215-241.
97. Reed, A. E.; Weinstock, R. B.; Weinhold, F., Natural population analysis. *The Journal of Chemical Physics* **1985**, 83 (2), 735-746.
-